Performance Comparison of Bearingless Motor Topologies in Exterior Rotor Construction

Thomas Reichert[1,a], Thomas Nussbaumer[2], Johann W. Kolar[1]

[1]Power Electronic Systems Laboratory, ETH Zurich, Switzerland

[2]Levitronix GmbH, Zurich, Switzerland

[a]reichert@lem.ee.ethz.ch

Abstract. This paper presents several feasible slot/pole combinations for a bearingless motor in exterior rotor construction. Due to the limited available stator space, the slot number of the stator has to be chosen small in order to provide sufficient winding space. The characteristics of each possible topology are discussed in great detail and for each setup the optimal design parameters are derived using 3D-FEM analysis. In the end, a fair comparison between the presented topologies is undertaken and the optimal motor topology is implemented in a real-size prototype setup.

Introduction

For the chemical, pharmaceutical and biotechnological industry sector, the qualitative refinement of high-purity mixing is a mandatory prerequisite to improve both research and production processes. State-of-the art mixing systems either use magnetic couplings or a long shaft passing through a seal to transmit the rotation energy from an outer motor into the process tank. With a bearingless motor [1-8], the common drawbacks of additional bearings inside the process tank and of pinch-off areas due to mechanical contact can be eliminated. Moreover, due to the large possible air gap, clean-in-place and sterilization-in-place processes [9] are facilitated. The bearingless motor is completely free of wear as well as free of lubrication and thus promises low maintenance cost and long life time.

The bearingless motor in exterior rotor construction can be advantageously employed for high-purity mixing when only the rotor is placed inside the process tank, whereas the stator and all control and power electronics are located outside, separated by the tank wall (cf. Fig. 1). The impeller can then be mounted directly onto the rotor, which levitates and rotates inside the tank in a contactless manner. With this construction type, flow-low zones are avoided and complete tank drainage through the bottom outlet is not disturbed. Moreover, high mixing torque can be produced with a compact setup.
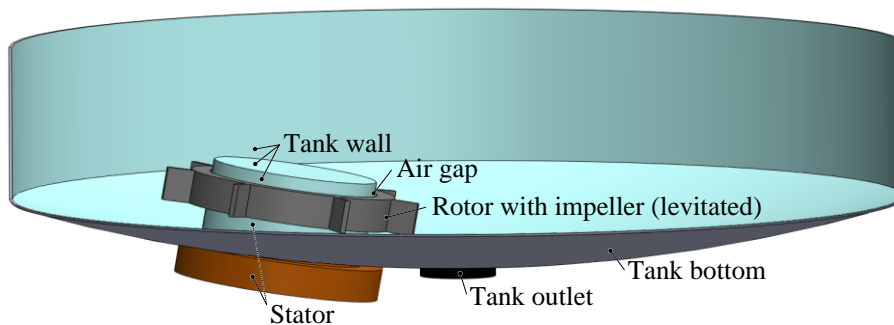

Fig. 1: Open view of the tank bottom. The stator is placed inside an indentation reaching into the tank bottom, but still outside of the tank wall. Only the rotor with the impeller blades is then mounted inside the process liquid and is levitated around the stator.

This paper will focus on different exterior rotor bearingless motor topology possibilities. In a first step, three feasible topologies are discussed and compared analytically. In a second step, their torque and bearing performances are compared based on a 3D-FEM analysis. The goal is to come up with high-torque motors that show stable bearing behavior under working conditions. In the end, the simulation results of the most promising topology are verified with the performance of prototype setup.

Exterior rotor bearingless motor topologies

The most characteristic topology differences for bearingless motors result from the choice of the rotor pole pair number p and the stator slot number q. Once this choice is made, mainly geometrical variations influence the final design of each motor.

For the exterior rotor construction type, the outer rotor diameter (which usually results from the required tank volume and the specific application) limits the motor size in the radial directions. Therefore, the stator space will be very limited since the whole stator iron and the windings need to be placed inside the hollow rotor ring. For this reason, only stator configurations with small slot numbers can be considered because the ratio of iron material to winding material would become unfavorably large otherwise. The proposed topologies are assembled with combined concentrated windings [10], so that there is one separate coil per stator tooth and it contributes to the generation of both torque and bearing forces. The required drive and bearing currents can be digitally controlled independent of each other and will then be superimposed mathematically prior to applying them to the stator coils. The rotor of the bearingless motor consists of a back iron ring and of permanent magnets which are magnetized in radial direction in alternating order.

With a very small slot number of three, a permanent magnet motor could be built. However, it is not possible to come up with a bearingless motor with this design, because drive and bearing would influence each other so that they cannot be controlled independently.

The four-slot/twelve-pole motor from Fig. 2(a) consists of a two-phase bearing combined with a single-phase drive. It can be controlled with an inverter consisting of four full-bridges,

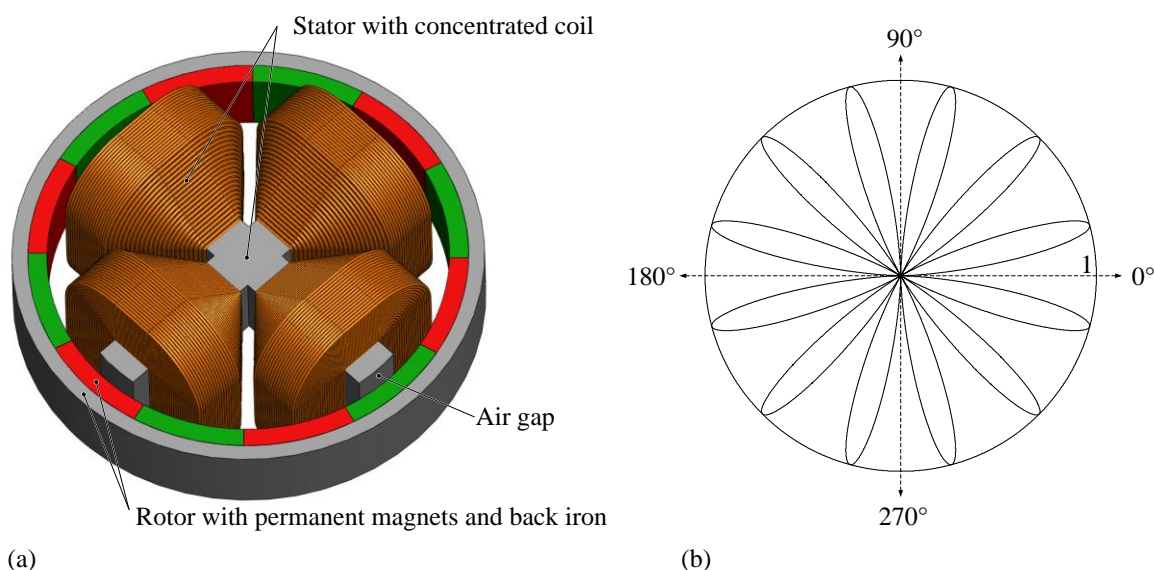(a)   (b)

Fig. 2: CAD drawing of a four-slot/twelve-pole motor topology in (a) and its torque characteristic in dependence on the rotor angle (when neglecting the cogging torque) in (b).

where each separated coil is controlled individually. The currents for both drive and bearing are superimposed and then applied independently to each coil. The reluctance force in the geometrical center position of the rotor is zero, thus only small bearing currents are required to stabilize the levitation. However, the drive produces a torque that varies over the rotation angle with the square of a sinusoidal function and thus even reaches zero for certain rotor angles. Moreover, a rather large cogging torque arises due to the non-fractional slot-pole-ratio. In Fig. 2(b), the (normalized) producible torque is shown in dependence on the rotor angle without consideration of the cogging torque. The bearing has to be fed with non-sinusoidal currents in order to create independent forces in *x*- and *y*-direction. It is possible to generate a constant force independent of the rotor angle, which would lead to a circle in the angular plot of Fig. 2(b).

The motor in Fig. 3(a) consists of a rotor with 16 permanent magnets and a five-slot stator. It is controlled by a five-phase bearing and a five-phase drive, which guarantees smooth drive torque. However, the control of this motor is challenging, because it cannot run with sinusoidal currents but rather with a complex function in order to decouple bearing and drive. Fig. 3(b) shows three of the five bearing currents for the generation of a force in *x*-direction. The calculation of these currents in the control is time consuming, which might lower the control performance. Moreover, high bearing currents have to be applied in order to stabilize the rotor in its center position due to non-zero reluctance forces appearing in dependence on the stator tooth width. This limits the available magnetomotive force for torque generation, when a certain maximum overall current density is maintained. When the currents are calculated correctly, is should be possible to generate drive and bearing forces that are independent of each other. This would lead to a circle in the angular plane, similar to Fig. 4(b) of the topology presented next. The cogging torque of this five-slot motor is very low due to the fractional slot-pole-ratio.

Fig. 4(a) shows a six-slot motor with a pole pair number of 8, which combines a three-phase bearing with a three-phase drive. It shows very low cogging torque and smooth drive torque. Moreover, the bearing requires low current because of a working point with zero reluctance force. For the control, two three-phase inverter stages are required, when one of the winding ends of three non-adjacent stator coils is connected to the three half-bridges, whereas the other winding ends are connected in star. In Fig. 4(b), the force generation in
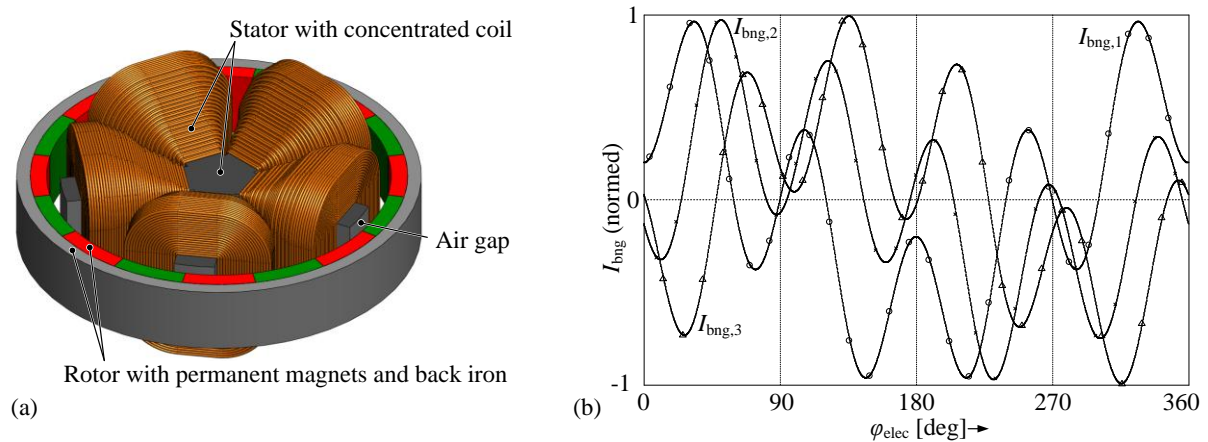

(a)

(b)

Fig. 3: CAD drawing of a five-slot/twelve-pole motor topology in (a) and three of the five bearing currents in dependence on the electrical angle in (b). It can be seen that the currents are not purely sinusoidal if drive and bearing forces have to be decoupled.

x-direction is shown for an excitation with a magnetomotive force of 1000 Ampere-turns (At), which is the product of the coil current and the winding number. When sinusoidal currents are applied, a constant force will result over the whole angular range. In Fig. 4(b), this is represented with a circle and confirmed with a 3D-FEM simulation.
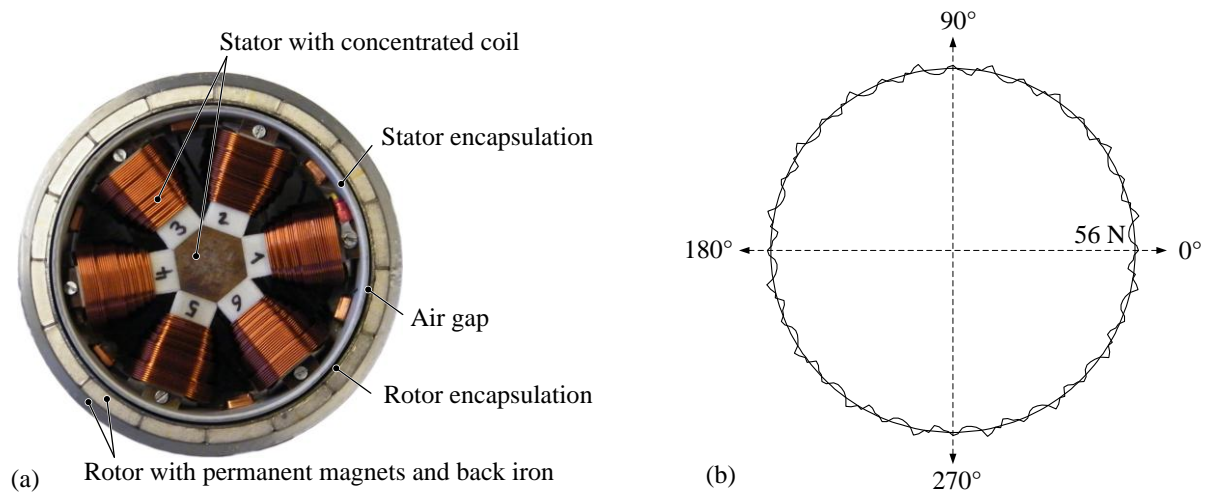

Fig. 4: Bearingless six-slot motor with a rotor consisting of 16 permanent magnets and a back iron ring. In (b), the force generation in *x*-direction is shown. Ideally, the force generation is constant and independent of the rotor angle when excited with sinusoidal currents, leading to a circle (dotted line) in this angular plot. This is confirmed with a 3D-FEM simulation (solid line), when a magnetomotive force of 1000 At is applied.

It would also be possible to come up with bearingless motor topologies that consist of stators with slot numbers of 8, 9, 10, 12 or even higher. These topologies will not be considered in this paper because of the aforementioned problem of the limited available stator space. Due to the large tooth number, these motors would fill up a large percentage of the area inside the hollow rotor with iron material, which would only allow the installation of small coils that could not produce sufficient magnetomotive force to generate a competitive torque output.

Comparison based on 3D-FEM analysis

The motor topologies described before have been analyzed using 3D-FEM simulations. In order to make a fair comparison, similar geometrical values have been chosen whenever possible. The outer rotor diameter (150 mm), the air gap length (5 mm) and the motor height (45 mm) are constant for all topologies. The rest of the geometrical values (in particular the stator diameter, the stator tooth width and the ratio of the radial length of back iron to permanent magnet) have been varied in a way to come up with high torque and stable bearing behavior. For the stator, only bar-shaped stator teeth without tooth tips were considered, because earlier simulations revealed saturation problems that lower the torque for more complex stator tooth shapes [11]-[12].

Both torque and bearing forces are produced when magnetomotive force is applied by means of energized stator coils. The magnetomotive force Θ can be stated as

$$\Theta = N_{\mathrm{coil}} \cdot I_{\mathrm{coil}} = J_{\mathrm{max}} \cdot A_{\mathrm{coil}} \; , \qquad\qquad (1)$$

where N_{coil} is the winding number and I_{coil} the applied current in that coil. It can be seen from (1) that the magnetomotive force in the stator coils is limited because a maximum current density J_{max} has to be respected due to thermal limits. For conventional air convection, 6 A/mm^2 shall not be exceeded whereas up to 25 A/mm^2 might be possible with additional water cooling. Obviously, the available winding area A_{coil} influences the maximum magnetomotive force as well. A trade-off has to be found between sufficient winding space (high magnetomotive force) and sufficient stator iron space (avoid heavy magnetic saturation).

In Fig. 5(a), the average torque output of the four-slot motor and the six-slot motor are compared for different combinations of magnet thickness and inner rotor diameter. This also determines the back iron length and the rotor diameter when respecting all the given constraints. A magnetomotive force with a peak value of 5000 At has been applied to the coils. For the four-slot motor, the peak value of the output torque would actually be twice the torque shown in Fig. 5(a), but the average torque is lower than for the six-slot motor. If there are similar torque values for different inner rotor diameter, it is recommendable to choose the largest diameter. This way, the stator can be built large as well, which will give the most possible space for windings. For the further analysis, the two options which are marked in Fig. 5(a) have been chosen.

In Fig. 5(b), the radial forces are shown for the four-slot and the six-slot topologies. In the center position (no radial deflection and no excitation currents), the resulting radial reluctance force is zero. When the rotor is moved away from its center position, a negative radial force is generated that would move the rotor even further away from its center position until it touches the stator. It can be seen that this negative force is stronger for the six-slot motor, so slightly higher control currents are required. With an excitation of 1000 At, a positive force can be generated that counteracts the negative reluctance force and brings the rotor back to its working point in the center.
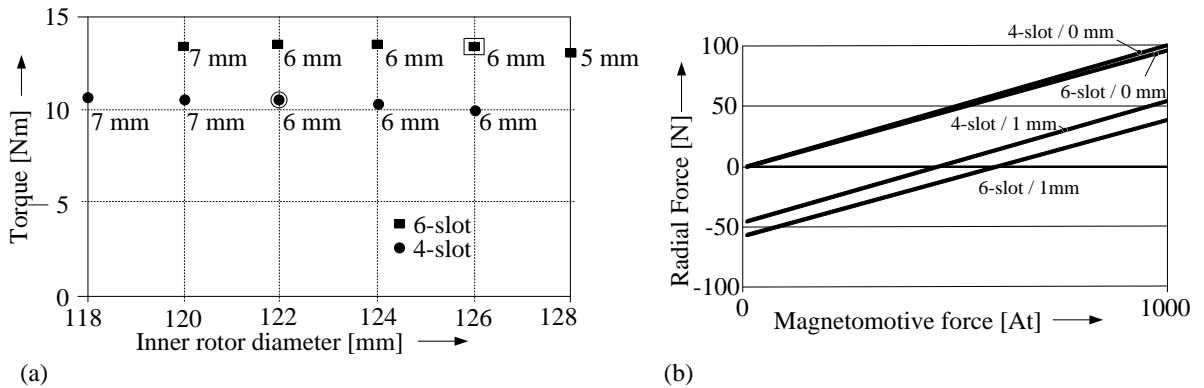

Fig. 5: In (a), the average torque output of the four-slot and the six-slot motor is compared. For an excitation with 5000 At, the inner rotor diameter and the magnet thickness are varied in order to come up with the highest torque. An analysis of the radial forces was undertaken in (b). It can be seen that both topologies have zero reluctance force in the center position. When the motors are displaced for 1 mm, the six-slot motor shows higher negative reluctance force. With an excitation of 1000 At, a similar positive restoring force can be generated for both topologies.

The cogging torque of the three different topologies has been analyzed in Fig. 6(a). For the five-slot and the six-slot motor, the cogging torque is very low and needs no further optimization. The cogging torque of the four-slot topology cannot be eliminated completely, so that there will always be an influence on the drive. Especially if low torque or low speed is required during a certain operation step, a jerky rotation might result. As a countermeasure to the cogging torque, the machine symmetry could be slightly disturbed, but this would also affect the drive output and the bearing.

Contrary to the other two topologies, the reluctance force of the five-slot motor in its center positions is not zero [cf. Fig. 6(b)]. There are resulting forces in x- and y-direction which show a sinusoidal dependence on the electrical rotation angle φ_{elec}, which is defined as the product of the mechanical rotation angle φ_{mech} and the rotor pole pair number p. With an optimal stator tooth width of 15 mm, the reluctance forces can be reduced to an acceptable minimum.

If the motor with a five-slot stator was implemented with a ball bearing, a constant torque of around 13 Nm over the whole angular range could result when a magnetomotive force of 5000 At is applied. However, the forces used for the torque generation also create unwanted resulting forces in the radial directions (in the range of 200 N). While these radial forces might be accepted with a ball bearing, it is impossible to run the motor with a magnetic bearing. For the bearingless motor, it is mandatory to decouple bearing forces and drive forces so a complex control is required that calculates the currents. The simulations revealed that the output torque is heavily lowered if the constraint of decoupled forces is respected. It was not possible to excite the coils (with an upper limit of 5000 At) in a way as to annihilate all radial forces and being able to generate torque that exceeds 5 Nm. Compared to the two other topologies, the five-slot bearingless motor is not compatible in terms of its torque output. Moreover, the aforementioned reluctance forces add another level of complexity to the control when a stable levitation shall be achieved.
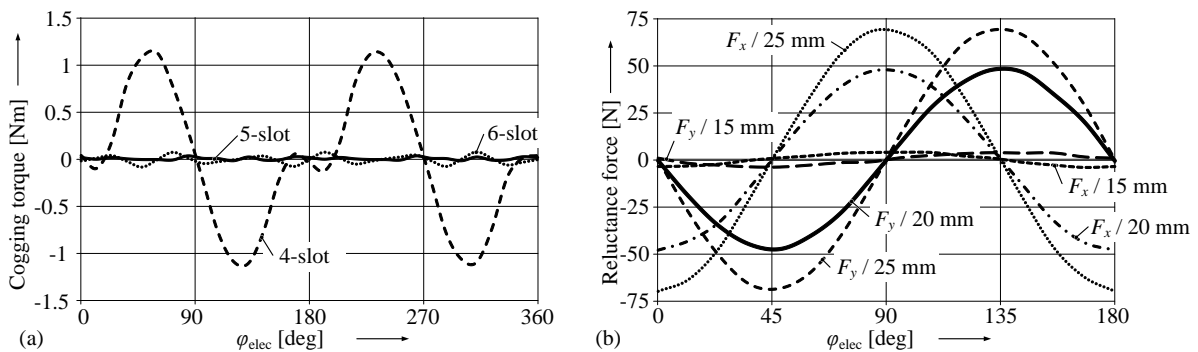

Fig. 6: The cogging torque can be neglected for the motor with five and six stator slots (b). For the four-slot motor, the cogging torque can be minimized but it will always be disturbing in the case of certain application steps with low torque or low speed, where it can lead to a jerky rotation. The reluctance force of the five-slot topology in its center position is depicted in (b) for different rotation angles and different tooth widths. It can be seen that the reluctance force can be minimized for a tooth width of 15 mm.

In Fig. 7(a), the two best options are compared in terms of their torque output when the excitation is varied. It can be seen that the six-slot topology can produce higher torque for the same maximum magnetomotive force (but with six coils instead of four). Another comparison can be undertaken when the torque in dependence on the maximum current density in the coils is compared. The four-slot topology has more winding space per coil

(around 1.5 times compared to the six-slot topology) since it only consists of four coils, so that a higher excitation is possible for the same maximum current density. It can be seen in Fig. 7(b) that the two topologies show similar torque output with a slight advantage for the four-slot topology.
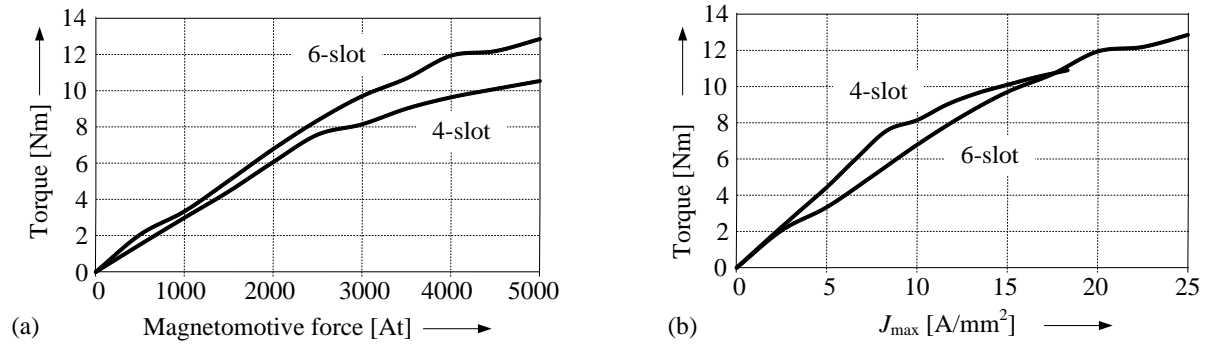

Fig. 7: Torque in dependence on the applied magnetomotive force (a) and in dependence on the maximum current density (b). It can be seen that the six-slot topology can produce higher torque for the same excitation (but with six coils instead of four). However, the space for windings is more limited than for the four-slot motor. Therefore, the comparison based on the maximum allowed current density is undertaken. It reveals that both motors show similar torque performance with a slight advantage for the four-slot topology.

Verification with prototype

The most promising topology with six stator teeth has been implemented in a real-size prototype setup and tested in a mixer environment. The outer rotor diameter was set to 150 mm and the optimal design parameters from Fig. 5(a) were considered. A prototype mixer head with four mixer blades was mounted onto the rotor and it was run in a water tank [cf. Fig. 8(a)]. The magnetic air gap is 5 mm, but the mechanical air gap is reduced to 1 mm due to thick rotor and stator encapsulation. The position measurement during mixing with 400 rpm in Fig. 8(b) reveals that the bearing is stable, since the rotor is not displaced for more than 200 μm from its center position.
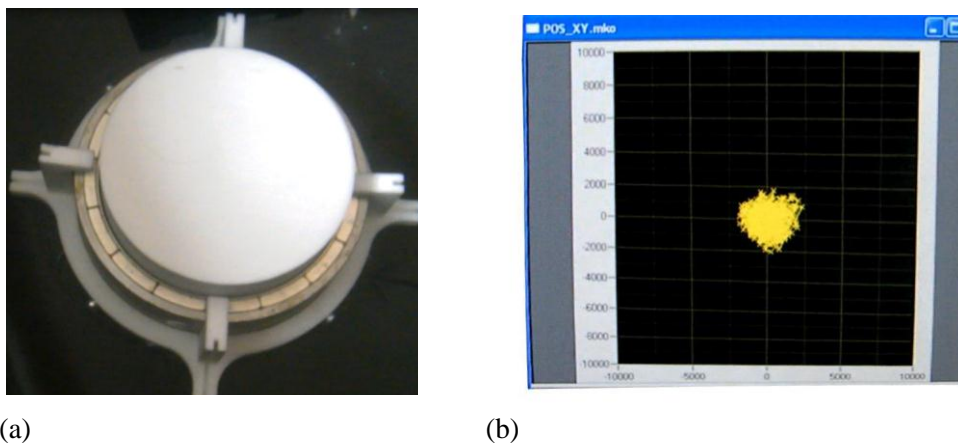

Fig. 8: A prototype was built of the six-slot motor and implemented into a water tank mixing setup (a). A test mixing head was mounted directly onto the rotor. During rotation with 400 rpm, the position was measured (b). The black square represents the mechanical air gap, which was only 1 mm for this setup due to thick rotor and stator encapsulations. It can be seen that the rotor movement is always below 20% of the air gap, which means that the rotor is never displaced for more than 200 μm despite the harsh working conditions.

Conclusions

The comparison of different bearingless motor topologies has been undertaken. It was shown, that a 4-slot/12-pole topology can provide very high peak torque but only offers an unfavorable single-phase drive characteristic with a moderate average torque. The 5-slot/16-pole topology cannot provide high torque when it is employed as a bearingless motor, since the drive should not create bearing forces. Moreover, the control effort is significantly higher and this motor would suffer from disturbing reluctance forces. A 6-slot/16-pole topology was found to be the most promising motor choice, due to stable bearing and drive over the whole angular range. Moreover, the control can be implemented with sinusoidal currents and it can be derived from field-oriented control. From the three compared topologies, the best average torque performance can be achieved. Therefore, the six-slot motor was implemented in a prototype and successfully run in a water tank setup.

References

[1] H. Sugimoto, K. Kamiya, R. Nakamura, J. Asama, A. Chiba, and T. Fukao, "Design and Basic Characteristics of Multi-Consequent-Pole Bearingless Motor With Bi-Tooth Main Poles," *IEEE Trans. Magn.*, vol. 45, no. 6, pp. 2791–2794, Jun. 2009.
[2] K. Raggl, B. Warberger, T. Nussbaumer, S. Burger, and J. W. Kolar, "Robust Angle-Sensorless Control of a PMSM Bearingless Pump," *IEEE Trans. Ind. Electron.*, vol. 56, no. 6, pp. 2076–2085, Jun. 2009.
[3] S.-M. Yang and M.-S. Huang, "Design and Implementation of a Magnetically Levitated Single-Axis Controlled Axial Blood Pump," *IEEE Trans. Ind. Electron.*, vol. 56, no. 6, pp. 2213–2219, Jun. 2009.
[4] S. Zhang and F. L. Luo, "Direct Control of Radial Displacement for Bearingless Permanent-Magnet-Type Synchronous Motors," *IEEE Trans. Ind. Electron.*, vol. 56, no. 2, pp. 542–552, Feb. 2009.
[5] T. Tera, Y. Yamauchi, A. Chiba, T. Fukao, and M. A. Rahman, "Performance of Bearingless and Sensorless Induction Motor Drive Based on Mutual Inductances and Rotor Displacements Estimation," *IEEE Trans. Ind. Electron.*, vol. 53, no. 1, pp. 187–194, Feb. 2006.
[6] R. Schoeb and N. Barletta, "Principle and Application of a Bearingless Slice Motor," *JSME Int. J. Series C,* vol. 40, pp. 593–598, 1997.
[7] M. Ooshima, A. Chiba, T. Fukao, and M. A. Rahman, "Design and Analysis of Permanent Magnet-Type Bearingless Motors," *IEEE Trans. Ind. Electron.*, vol. 43, no. 2, pp. 292–299, Apr. 1996.
[8] S. Silber, W. Amrhein, P. Bösch, R. Schoeb, and N. Barletta, "Design aspects of bearingless slice motors," *IEEE/ASME Trans. Mechatronics*, vol. 10, no. 6, pp. 611–617, Dec. 2005.
[9] Y. Christi and M. Moo-Young, "Clean-in-place systems for industrial bioreactors: Design, validation and operation," *Journal of Industrial Microbiology and Biotechnology,* vol. 13, no. 4, pp. 201–207, Jul. 1994.
[10] K. Raggl, T. Nussbaumer, and J. W. Kolar, "Comparison of Separated and Combined Winding Concepts for Bearingless Centrifugal Pumps", *Journal of Power Electronics*, vol. 9, no. 2, pp. 243–258, 2009.
[11] P. Karutz, T. Nussbaumer, W. Gruber, and J. W. Kolar, "Acceleration-Performance Optimization for Motors With Large Air Gaps," *IEEE Trans. Ind. Electron.*, vol. 57, no. 1, pp. 52–60, Jan. 2010.
[12] P. Karutz, T. Nussbaumer, W. Gruber, and J. W. Kolar, "Saturation Effects in High Acceleration Bearingless Slice Motors, " Proc. of the 2008 *IEEE International Symposium on Industrial Electronics*, pp. 472–477, 2008.